PHYSICAL REVIEW E **89**, 060502(R) (2014)

Self-assembly of skyrmion-dressed chiral nematic colloids with tangential anchoring

M. B. Pandey,[1,2] T. Porenta,[3] J. Brewer,[1] A. Burkart,[1] S. Čopar,[3,4] S. Žumer,[3,4] and Ivan I. Smalyukh[1,5,6,*]

[1]*Department of Physics and Liquid Crystal Materials Research Center, University of Colorado, Boulder, Colorado 80309, USA*

[2]*Department of Physics, VSSD College, Kanpur 208 002, India*

[3]*Faculty of Mathematics and Physics, University of Ljubljana, Jadranska 19, 1000 Ljubljana, Slovenia*

[4]*Jozef Stefan Institute, Jamova 39, 1000 Ljubljana, Slovenia*

[5]*Department of Electrical, Computer, and Energy Engineering and Materials Science and Engineering Program, University of Colorado, Boulder, Colorado 80309, USA*

[6]*Renewable and Sustainable Energy Institute, National Renewable Energy Laboratory and University of Colorado, Boulder, Colorado 80309, USA*

(Received 6 May 2014; published 30 June 2014)

We describe dipolar nematic colloids comprising mutually bound solid microspheres, three-dimensional skyrmions, and point defects in a molecular alignment field of chiral nematic liquid crystals. Nonlinear optical imaging and numerical modeling based on minimization of Landau–de Gennes free energy reveal that the particle-induced skyrmions resemble torons and hopfions, while matching surface boundary conditions at the interfaces of liquid crystal and colloidal spheres. Laser tweezers and videomicroscopy reveal that the skyrmion-colloidal hybrids exhibit purely repulsive elastic pair interactions in the case of parallel dipoles and an unexpected reversal of interaction forces from repulsive to attractive as the center-to-center distance decreases for antiparallel dipoles. The ensuing elastic self-assembly gives rise to colloidal chains of antiparallel dipoles with particles entangled by skyrmions.

DOI: 10.1103/PhysRevE.89.060502 PACS number(s): 61.30.Jf, 61.30.Mp

Anisotropic self-assembly of mesoscopic colloidal structures is important both fundamentally and technologically and is typically achieved by exploiting the anisotropies of interactions due to the particles themselves, e.g., arising from a nonspherical shape and patched surface functionalization, or mediated by the surrounding host medium, or utilizing both of these mechanisms simultaneously [1–12]. Liquid crystals (LCs) are promising host media for reconfigurable self-assembly of colloidal particles [4]. Particles embedded in these structured media induce defects and interact with each other via elasticity-mediated forces [4,5] arising to minimize the free energy cost of elastic distortions and defects. Electrostatic analogies in the structure and interactions of nematic colloids allowed for understanding the physical underpinnings behind many experimental observations [4–8]. Both dipolar and quadrupolar nematic colloids form in the case of perpendicular surface boundary conditions on particle surfaces [4,5,8], but only quadrupolar-symmetry structures were observed for particles with tangential boundary conditions and only point and ring-shaped line defects could be induced [8].

In this Rapid Communication, we demonstrate that a host of unusual elastic colloidal configurations and self-assembled structures arise in a uniformly aligned LC when a small amount of chiral agent is added, while also imposing perpendicular boundary conditions on the confining surfaces, so that the system is frustrated by being unable to realize twisted configurations. The particles locally relieve this frustration by enabling twist through inducing skyrmionic configurations that resemble torons and hopfions [13,14]. In homeotropic cells, these skyrmion-colloidal hybrids align with dipolar axes perpendicular to confining cell substrates and parallel or antiparallel to each other. Parallel elastic dipoles exhibit purely repulsive pair interactions, but interactions of antiparallel dipoles, unexpectedly, reverse from repulsive to attractive as the center-to-center distance decreases. The ensuing elasticity self-assembly can be tuned to yield long-range repulsive interactions, or, more interestingly, self-assembly of antiparallel dipolar colloidal chains with skyrmionic field configurations entangling the particles. Using a combination of nonlinear optical imaging, laser tweezers [15], videomicroscopy, and numerical modeling, we probe and explain the physical underpinnings behind these interactions based on considerations of symmetry, LC elasticity, and chirality.

A chiral nematic LC (CNLC) with desired cholesteric pitch was obtained by doping a nematic host AMLC-0010 (from AlphaMicron, Inc.) with chiral additive S-811 (EM Chemicals) [13]. The CNLC was mixed with a powder of melamine resin microspheres of diameter $\sim 7\ \mu$m (Fluka Chemicals) obtained from an aqueous dispersion by slow water evaporation. These particles impose tangential degenerate surface boundary conditions on the director **n** describing the local average LC molecular orientation. To fabricate cells, glass plates were washed with Alconox detergent in the supersonic bath for 2 h and then rinsed with de-ionized water, acetone, and isopropyl alcohol. Strong perpendicular boundary conditions on the inner surfaces of the confining glass plates were set by treating them via dip coating in a 1 wt% aqueous solution of *N*,*N*-dimethyl-*n*-octadecyl-3-aminopropyltrimethoxysilyl chloride (DMOAP). These plates were then glued together using UV-curable glue mixed with 10 μm spacers to define the cell gap of about 10 μm. The cells were infiltrated with CNLC colloidal dispersions and sealed using epoxy glue. They were probed using a polarizing optical microscope (POM) and three-photon excitation fluorescence polarizing microscopy (3PEF-PM) [15]. Using holographic optical tweezers (HOTs) [15], particles were moved with respect to each other to set initial conditions and measure interaction forces. Using

*Corresponding author: ivan.smalyukh@colorado.edu

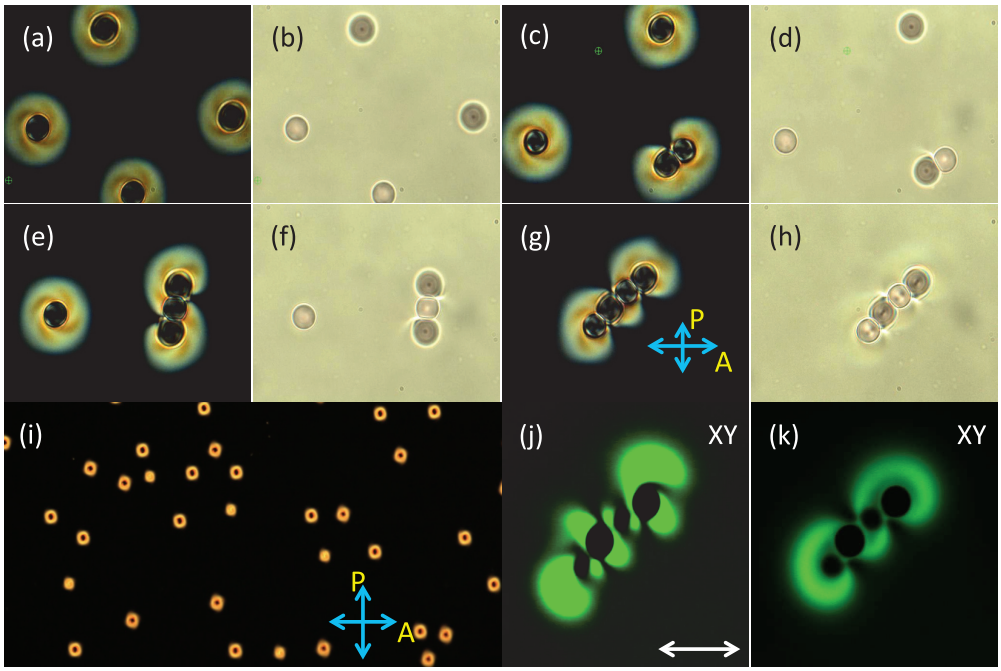

FIG. 1. (Color online) Particles with tangential surface anchoring dispersed in an unwound CNLC. Individual particles [(a), (b)] are released in proximity to each other using laser tweezers and prompted to interact while forming colloidal [(c), (d)] dimers, [(e), (f)] trimers, and [(g), (h), (j), (k)] tetramers. The colloidal configurations and director structures are studied [(a), (c), (e), (g), (i)] between crossed polarizers in POM, [(b), (d), (f), (h)] using bright-field optical microscopy, and [(j), (k)] using 3PEF-PM cross sections such as the one shown for a horizontal plane slightly above the cell midplane. Orientations of crossed polarizers in POM are depicted in (g) and (i). 3PEF-PM polarization is linear in (j), as marked by a white double arrow, and circular in (k). The particle diameter is 7 μm.

videomicroscopy and IMAGEJ tracking software, we extracted center-to-center particle separation versus time data with a 5–10 nm precision.

Optical manipulations and three-dimensional (3D) imaging of samples were performed with an integrated setup of HOTs and 3PEF-PM built around an inverted microscope IX 81 (Olympus) and using an oil-immersion 100 × objective with a numerical aperture of 1.4. HOTs utilized a phase-only spatial light modulator (Boulder Nonlinear Systems) and an ytterbium-doped fiber laser (IPG Photonics) operating at 1064 nm [15]. 3PEF-PM imaging employed a tunable Ti-sapphire oscillator (680–1080 nm, from Coherent) emitting 140 fs pulses at a repetition rate of 80 MHz, and a photomultiplier tube detector H5784-20 (Hamamatsu) [15]. 3D resolution of the 3PEF-PM (about 500 nm) is enabled by nonlinear optical excitation and strong ($\propto \cos^6\theta$) dependence of fluorescence on the angle θ between $\mathbf{n}(\mathbf{r})$ and the linear polarization of excitation light. Maximum- and minimum-intensity areas of 3PEF-PM textures have LC molecules and $\mathbf{n}(\mathbf{r})$ parallel and perpendicular to linear polarization of the excitation light, respectively. Additionally, 3PEF-PM images obtained with circularly polarized excitation light have bright regions where $\mathbf{n}(\mathbf{r})$ lies in the sample plane.

Using cells with wedge geometry and dihedral angles of 1°–3°, we have varied the local cell thickness d. We observed unwound vertically aligned director structures for thickness-pitch ratios up to $d/p \approx 0.75$, where p is the equilibrium pitch of the CNLC. Individual localized cholesteric fingers and other structures are commonly observed at $d/p \approx 0.75$–1. When dispersed in frustrated confined CNLCs with d/p up to about 0.6, particles with tangential anchoring induce $\mathbf{n}(\mathbf{r})$ structures with quadrupolar symmetry having two boojums at the poles along the vertical far-field director, as previously observed for nonchiral LCs [8]. Different types of particle-induced structures are observed for $d/p \approx 0.75$–1, which in POM micrographs appear as doughnut-shaped bright rings (Fig. 1) and will be the focus of our present study. In the intermediate range of $d/p \approx 0.6$–0.75, these skyrmionic configurations around some of the particles coexist with the conventional quadrupolar $\mathbf{n}(\mathbf{r})$ structures accompanying other particles.

Optical micrographs shown in Figs. 1(a), 1(b), and 1(i) reveal CNLC colloidal dispersions of well-separated particles accompanied by localized doughnut-shaped birefringent $\mathbf{n}(\mathbf{r})$ structures. These particles can levitate at two different depth levels, below and above the cell's midplane, as observed by refocusing the microscope [Figs. 1(b), 1(d), 1(f), and 1(h)]. Brushes in doughnut-shaped birefringent rings around particles have spiraling directions dependent on whether the particle center resides above or below the cell midplane. By releasing particles at different separations, optical manipulation reveals that particles centered at the same depth level interact repulsively at all center-to-center distances ranging up to six particle diameters, at which the strength of elastic repulsion becomes comparable to that of Brownian motion. On the other hand, particles at different depth levels repel only at large distances but attract at short distances, leading to the formation of colloidal dimers [Figs. 1(c) and 1(d)]. Additional particles join the dimer [Figs. 1(e)–1(h)] to form trimers, tetramers, etc. Importantly, interaction of the ensuing chains with individual particles is highly anisotropic and selective

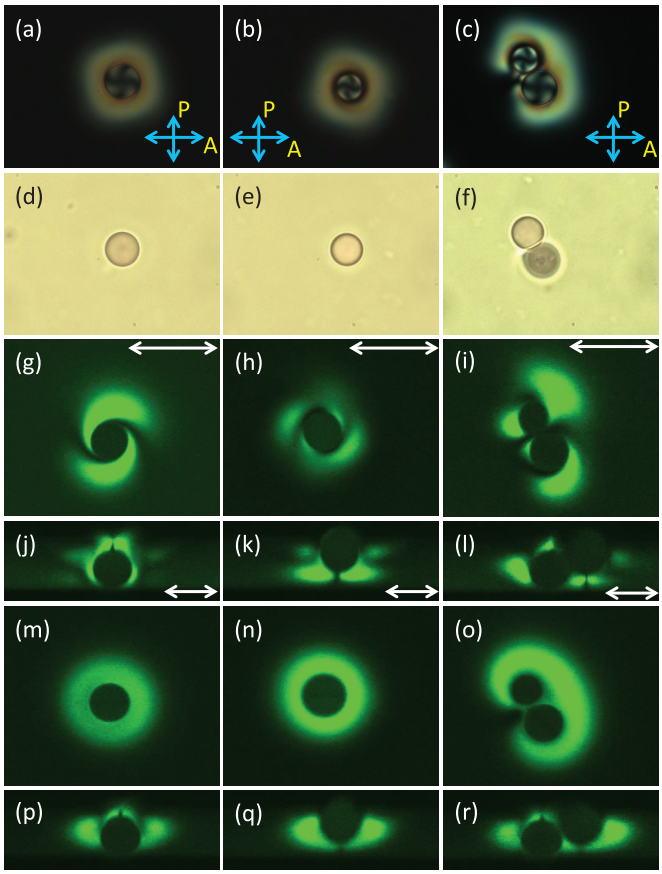

FIG. 2. (Color online) 3D imaging of **n**(**r**) induced by individual particles and dimers formed by two antiparallel elastic dipoles. [(a), (b)] POM and [(d), (e)] bright-field micrographs of two individual elastic dipoles, and [(c), (f)] their self-assembled dimer. Bright-field images [(d)–(f)] indicate that the particles might be located at different depths within the sample. [(g)–(i), (m)–(o)] In-plane and [(j)–(l), (p)–(r)] vertical 3PEF-PM cross sections obtained with [(g)–(l)] linearly and [(m)–(r)] circularly polarized excitation light.

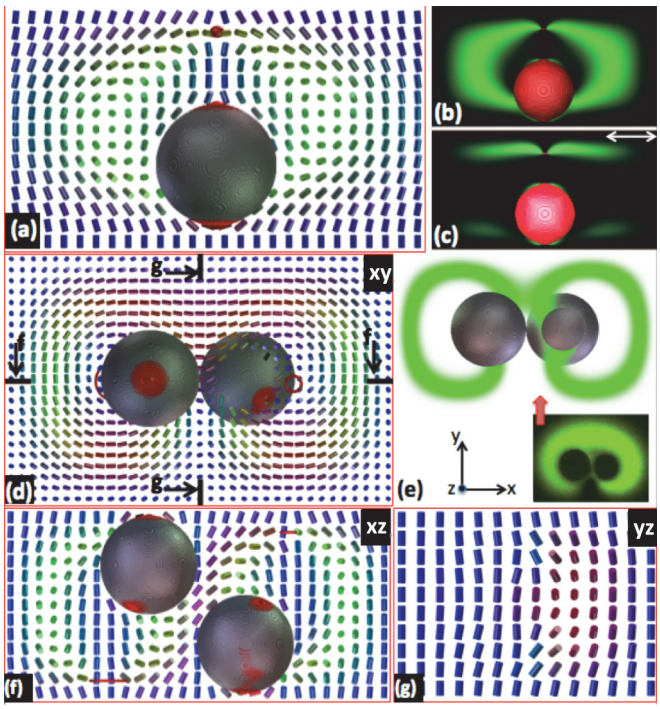

FIG. 3. (Color online) Computer-simulated director configurations induced by colloidal spheres with tangential anchoring. (a) Axially symmetric dipolar **n**(**r**) in the cell's vertical cross-section. (b), (c) Computer-simulated 3PEF-PM textures in the same cross section (b) for circularly and (c) linearly polarized probing light. (d)–(g) Computer-simulated **n**(**r**) of self-assembled colloidal dimers as depicted (d) in the in-plane x-y cross section in the cell midplane and (f), (g) vertical cross sections in two perpendicular planes marked in (d). (e) Computer-simulated 3PEF-PM image for circularly polarized excitation light and **n**(**r**) shown in (d); the inset shows the corresponding experimental image. The red (dark gray), green (bright gray), and blue (gray) coloring of cylinders in (a), (d), (f), and (g) indicates director projections along the three coordinate directions x, y, and z, respectively. Regions of defects with reduced scalar order parameter are shaded in red (dark gray). Note that the induced bulk and surface defects of a particle dimer shown in (d) and (f) shift away from vertical axes passing through the particle'scenters.

so that it always leads to alternation of the depth location of the particles joining the chains. POM [Figs. 1(a), 1(c), 1(e), and 1(g)] and 3PEF-PM [Figs. 1(j), 1(k), and 2] [15] textures have low symmetry. Dipolar CNLC colloids do not preserve their axially symmetric structure upon self-assembly, but rather morph to multiparticle chains entangled by twisted **n**(**r**) structures (Fig. 1). To elucidate the nature of this type of organization, we obtain detailed 3PEF-PM images of individual colloidal particles and particle self-assemblies (Fig. 2). 3D imaging confirms spontaneous dipolar symmetry breaking in the particle-induced **n**(**r**) and reveals that the particles are shifted either upward or downward with respect to the cell midplane while inducing elastic dipoles pointing either upward or downward [Figs. 2(g), 2(h), 2(j), and 2(k)]. Colloidal dimers are formed by pairs of antiparallel elastic dipoles bound together by twisted **n**(**r**) [Figs. 2(c), 2(f), 2(i), 2(l), 2(o), and 2(r)]. This antiparallel up-down orientation of neighboring elastic dipoles is also characteristic of colloidal trimers, tetramers, and longer chains (Fig. 1).

Experimental **n**(**r**) was compared to a numerical model. We used the numerical finite difference relaxation method to minimize the Landau–de Gennes free energy with a single elastic constant and a chiral term for $d/p = 0.85$ [9,12,16]. The free energy and elastic constants are adopted from Ref. [17]. The simulated **n**(**r**) around single particles and dimers are consistent with experiments (Fig. 3). To illustrate this, we have used the minimum-energy axially symmetric **n**(**r**) shown for the vertical cross section in Fig. 3(a) to computer simulate the corresponding 3PEF-PM images for both linearly and circularly polarized excitation light. Despite the fact that modeling does not account for finite resolution effects [15], computer-simulated and experimental images resemble each other [compare Figs. 3(b) and 3(c) and Figs. 2(k) and 2(q) while noting the reversed dipole orientations]. In a similar way, a good agreement is also found for simulated and experimental **n**(**r**) induced by colloidal dimers [Figs. 3(d) and 3(e)] and other self-assemblies. The particle-induced configuration contains a bulk defect (a hyperbolic hedgehog point defect or a small disclination loop of elementary topological hedgehog charge ± 1, where the sign can be positive or negative, depending on the

direction of the vector field lines decorating the director field [10]) and two boojums at the poles of a melamine resin particle along the cell normal [Fig. 3(a)]. The requirement of topological charge conservation dictates that the total hedgehog charge of a spherical particle with two boojums and a looped double-twist cylinder of $\mathbf{n}(\mathbf{r})$ is ± 1, compensating that of the bulk point defect. The topological hedgehog charge of a looped double-twist cylinder is zero [14,18], meaning that the particle with two boojums and nonuniform $\mathbf{n}(\mathbf{r})$ on its surface has a hedgehog charge of ± 1, consistent with results of our topological and numerical modeling discussed in detail elsewhere [19].

The bulk defect can localize above or below the microsphere, determining the elastic dipole's direction. In addition to these bulk and surface defects, the particle is surrounded by a double-twist cylinder of $\mathbf{n}(\mathbf{r})$ looped on itself. Such double-twist cylinders are building blocks of cholesteric blue phases and also rather familiar to condensed matter community two-dimensional skyrmions, smooth field configurations that are associated with topological numbers, similar to more conventional singular defects [14]. A closed loop of the double-twist cylinder is the basis of a three-dimensional skyrmion, also known as a hopfion [14] and referred to as "texture" in cosmology [20]. The nematic ground state manifold $\mathbf{R}P^2$ is a sphere with antipodal points identified, and these two- and three-dimensional skyrmions are labeled by elements of the second and third homotopy groups, $\pi_2(\mathbf{R}P^2) = \boldsymbol{Z}$ and $\pi_3(\mathbf{R}P^2) = \boldsymbol{Z}$, respectively, defects not observed in nematic colloids in the past. Previously, hopfions and torons homeomorphic to them could be generated in CNLCs by vortex laser beams [13,14]. The present study shows that colloidal particles can also induce hopfions and torons, the existence of which is prompted by the chirality of the CNLC. Previously LC colloids were found inducing only boojums, bulk point defects (hyperbolic hedgehogs), and disclination rings [4,5,8,21–29]. Although our structure has dipolar symmetry, similar to the classic one formed by a particle and a point defect [4], it contains a hopfion induced by the particle, as well as bulk and surface point defects at the same time. Furthermore, it contrasts previous studies by the fact that dipolar structures were not formed by particles with tangential anchoring as well as hopfions, boojums, and bulk point defects at the same time. Importantly, this leads to highly unusual interactions between colloidal particles, as we demonstrate below.

To probe pair interactions, we assume that the motion of particles entails no changes in $\mathbf{n}(\mathbf{r})$ configurations translating along with them (small Ericksen numbers) [8,10,12]. This motion is also highly overdamped (Reynolds number $\ll 1$) [12], and we therefore neglect inertia effects, assuming that elasticity-mediated interaction forces are balanced by the viscous Stokes drag forces [1], $F_{\text{drag}} = -\zeta dR/dt$, where ζ is a drag coefficient. We determine ζ by probing the diffusive motion of a single particle in the confined CNLC with videomicroscopy under identical conditions. Histograms sampled from the time-delayed particle displacements are described by Gaussian distributions with mean-squared displacements that are linear in elapsed time, with the slope corresponding to the diffusivity D in the lateral plane of the sample, which is the same in all directions in the plane of the cell because of the vertical far-field alignment [6]. We then calculate the viscous drag coefficient from an experimentally determined

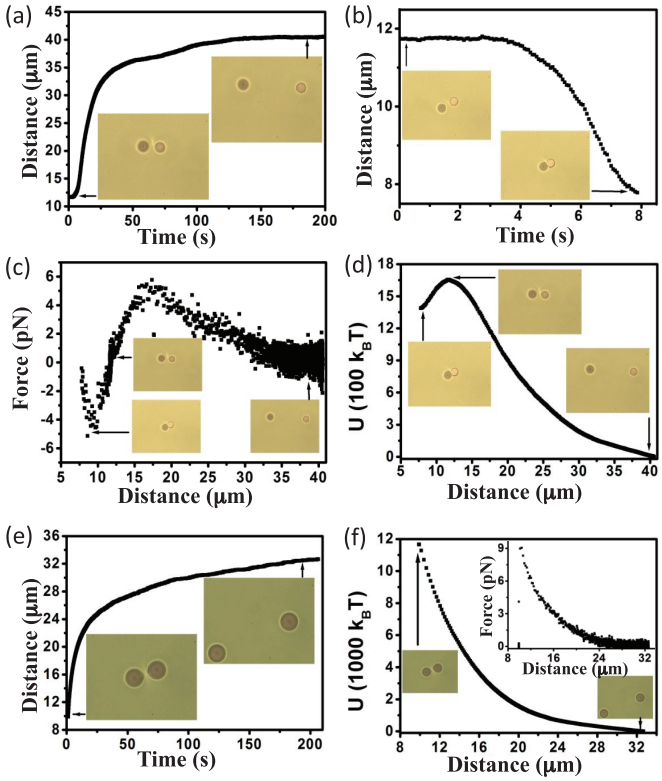

FIG. 4. (Color online) Colloidal pair interactions. (a), (b) Center-to-center distance vs time dependencies probed by videomicroscopy for antiparallel orientation of elastic dipoles when released by laser tweezers at an initial separation (a) just above and (b) just below the critical distance r_c, at which the pair-interaction force changes from repulsive to attractive. (c) Pair-interaction force and (d) potential obtained from data similar to those shown in (a) and (b). (e) Particle center-to-center distance vs time for parallel elastic dipoles released by laser tweezers at the smallest achievable separation. (f) Pair-interaction potential and force (shown in the inset) obtained from data similar to those shown in (e). Insets in (a)–(f) show bright-field optical micrographs taken at initial and final distances of the corresponding dependencies.

diffusion constant using the Einstein relation $\zeta = k_B T/D = 2.366 \times 10^{-6}\,\text{N s/m}$, where $k_B = 1.38 \times 10^{-23}\,\text{J/K}$ is Boltzmann's constant and T is the absolute temperature [6]. This force balance reveals distance dependencies of interaction forces between differently aligned elastic dipoles, which are then used to obtain pair-interaction potentials (Fig. 4). Colloidal particles with both parallel and antiparallel orientation of the elastic dipoles interact repulsively at large distances. However, at short distances, antiparallel elastic dipoles attract. At a certain critical center-to-center separation r_c with a maximum pair-interaction potential [Fig. 4(d)], the pair-interaction force flips from repulsive at large distances to attractive at short distances [Fig. 4(c)]. Particles with parallel elastic dipoles mutually repel at all distances [Figs. 4(e) and 4(f)].

The observed colloidal pair interactions are highly unusual for nematic colloids because of the reversal of interparticle forces from repulsive to attractive (Fig. 4), which occurs despite the existence of equilibrium separation between particles at a center-to-center distance of about $2.5R$ [Figs. 3(f) and 4(c)]. Although elastic interactions between nematic

colloids are often described by the electrostatic analogy and multipole expansion of the interaction potential, this approach cannot be applied directly in our case. Since the symmetry axes of field configurations due to individual colloidal particles are normal to cell substrates, elastic dipoles align perpendicular to confining surfaces, too, and point upward or downward [Fig. 3(a)]. Naively, one would expect attractive interactions for antiparallel dipoles and repulsive interactions for parallel ones at all distances. However, the antiparallel dipoles are found to repel at large distances and attract only at short distances, which can be qualitatively understood by considering the particle-induced $\mathbf{n}(\mathbf{r})$ [Fig. 3(a)]. Despite the asymmetry in the particle and bulk point defect positions forming a dipolar near-field $\mathbf{n}(\mathbf{r})$, the structure is seen as a single toron or hopfion from a long distance. The distortions in the exterior are fairly symmetric with respect to the cell midplane [Fig. 3(a)] because the double-twist cylinder loops around the dipole and screens the elastic dipole moment of the overall particle-toron hybrid, making the long-distance interactions quadrupolarlike (although further screened by the cell confinement), i.e., always repulsive in our geometry. At short distances comparable to the size of the particle-toron hybrid, the double-twist portions of the solitons start to interpenetrate, and the symmetry breaking in the interior of this configuration starts playing a role, leading to short-range attractive interactions and the eventual formation of dimers and chains with antiparallel dipoles, in which the particles are found entangled by meanders of the two-dimensional skyrmions (Figs. 1–3). This behavior cannot simply arise from an interplay between the dipole and quadrupole terms in the effective interparticle interaction of nematic colloids without a chiral additive and is caused by the highly unusual "screening" of structural asymmetry by the skyrmion surrounding the particles.

To conclude, we have developed a nematic colloidal system with particle-toron hybrid structures and unusual pair interactions, which are found to be repulsive at long distances but attractive at short distances comparable to toron dimensions. These interactions lead to well-defined colloidal self-assemblies in the forms of both low-symmetry colloidal chains and various lattices that can self-organize due to long-range weakly anisotropic repulsive interactions and can be potentially tuned and selected by applying fields. Our study demonstrates that, in addition to symmetry [2,4–10], molecular chirality [22,23], and applied field [24,25–29], localized topological skyrmionic field configurations, such as torons and hopfions, can be utilized in designing mesoscale self-assembly of colloidal particles and stable topological defects in LCs.

We acknowledge discussions with P. J. Ackerman and B. Senyuk. This work was supported by the NSF Grant No. DMR-0847782 (J.B., A.B., I.I.S), DOE Grant No. ER46921 (I.I.S.), as well as the NAMASTE Center of Excellence and Slovenian Research Agency Contracts No. P1-0099 and No. J1-2335 (S.Č., T.P., S.Ž.). M.B.P. acknowledges support of the Indian Government through the DST-BOYSCAST Fellowship program.

[1] R. J. Hunter, *Foundations of Colloid Science* (Oxford University Press, New York, 2001).
[2] B. Senyuk, J. S. Evans, P. Ackerman, T. Lee, P. Manna, L. Vigderman, E. R. Zubarev, J. van de Lagemaat, and I. I. Smalyukh, Nano Lett. **12**, 955 (2012).
[3] O. E. Semonin, J. M. Luther, S. Choi, H.-Y. Chen, J. Gao, A. J. Nozik, and M. C. Beard, Science **334**, 1530 (2011).
[4] P. Poulin, H. Stark, T. C. Lubensky, and D. A. Weitz, Science **275**, 1770 (1997).
[5] T. C. Lubensky, D. Pettey, N. Currier, and H. Stark, Phys. Rev. E **57**, 610 (1998).
[6] C. Lapointe, T. Mason, and I. I. Smalyukh, Science **326**, 1083 (2009).
[7] U. Tkalec, M. Škarabot, and I. Muševič, Soft Matter **4**, 2402 (2008).
[8] P. Poulin and D. A. Weitz, Phys. Rev. E **57**, 626 (1998).
[9] M. Škarabot, M. Ravnik, S. Žumer, U. Tkalec, I. Poberaj, D. Babič, N. Osterman, and I. Muševič, Phys. Rev. E **77**, 031705 (2008).
[10] B. Senyuk, Q. Liu, S. He, R. D. Kamien, R. B. Kusner, T. C. Lubensky, and I. I. Smalyukh, Nature (London) **493**, 200 (2013).
[11] A. M. Alsayed, M. F. Islam, J. Zhang, P. J. Collings, and A. G. Yodh, Science **309**, 1207 (2005).
[12] P. M. Chaikin and T. C. Lubensky, *Principles of Condensed Matter Physics* (Cambridge University Press, Cambridge, U.K., 2000).
[13] I. I. Smalyukh, Y. Lansac, N. Clark, and R. Trivedi, Nat. Mater. **9**, 139 (2010).
[14] B. Gin-ge Chen, P. J. Ackerman, G. P. Alexander, R. D. Kamien, and I. I. Smalyukh, Phys. Rev. Lett. **110**, 237801 (2013).
[15] R. P. Trivedi, T. Lee, K. A. Bertness, and I. I. Smalyukh, Opt. Express **18**, 27658 (2010).
[16] M. Ravnik and S. Žumer, Liq. Cryst. **36**, 1201 (2009).
[17] M. Ravnik, M. Škarabot, S. Žumer, U. Tkalec, I. Poberaj, D. Babič, N. Osterman, and I. Muševič, Phys. Rev. Lett. **99**, 247801 (2007).
[18] J. S. Evans, P. J. Ackerman, D. J. Broer, J. van de Lagemaat, and I. I. Smalyukh, Phys. Rev. E **87**, 032503 (2013).
[19] T. Porenta, S. Čopar, P. J. Ackerman, M. B. Padney, M. C. M. Varney, I. I. Smalyukh, and S. Žumer (unpublished).
[20] N. Turok, Phys. Rev. Lett. **63**, 2625 (1989).
[21] S. Čopar, T. Porenta, and S. Žumer, Liq. Cryst. **40**, 1759 (2013).
[22] V. S. R. Jampani, M. Škarabot, S. Čopar, S. Žumer, and I. Muševič, Phys. Rev. Lett. **110**, 177801 (2013).
[23] R. P. Trivedi, I. I. Klevets, B. Senyuk, T. Lee, and I. I. Smalyukh, Proc. Natl. Acad. Sci. USA **109**, 4744 (2012).
[24] A. Nych, U. Ognysta, M. Škarabot, M. Ravnik, S. Žumer, and I. Muševič, Nat. Commun. **4**, 1489 (2013).
[25] G. P. Alexander, B. G. Chen, E. A. Matsumoto, and R. D. Kamien, Rev. Mod. Phys. **84**, 497 (2012).
[26] Y. Gu and N. L. Abbott, Phys. Rev. Lett. **85**, 4719 (2000).
[27] O. V. Kuksenok, R. W. Ruhwandl, S. V. Shiyanovskii, and E. M. Terentjev, Phys. Rev. E **54**, 5198 (1996).
[28] H. Stark, Eur. Phys. J. B **10**, 311 (1999).
[29] J. C. Loudet and P. Poulin, Phys. Rev. Lett. **87**, 165503 (2001).